Autonomic neurocristopathy-associated mutations in PHOX2B dysregulate *Sox10* expression

Mayumi Nagashimada,[1,2] Hiroshi Ohta,[3] Chong Li,[3] Kazuki Nakao,[4] Toshihiro Uesaka,[1] Jean-François Brunet,[5] Jeanne Amiel,[6] Delphine Trochet,[6] Teruhiko Wakayama,[3] and Hideki Enomoto[1,2]

[1]Laboratory for Neuronal Differentiation and Regeneration, RIKEN Center for Developmental Biology, Kobe, Japan. [2]Department of Development and Regeneration, Graduate School of Medicine, Osaka University, Osaka, Japan. [3]Laboratory for Genomic Reprogramming and [4]Laboratory for Animal Resources and Genetic Engineering, RIKEN Center for Developmental Biology, Kobe, Japan. [5]Institut de Biologie de l'École Normale Supérieure (IBENS), CNRS UMR8197, INSERM U1024, and Labex MemoLife, Paris Science et Lettres Research University, Paris, France. [6]INSERM U781 et Département de Génétique, Hôpital Necker-Enfants Malades, Université Paris Descartes, Faculté de Médecine, Assistance Publique-Hopitaux de Paris (AP-HP), Paris, France.

The most common forms of neurocristopathy in the autonomic nervous system are Hirschsprung disease (HSCR), resulting in congenital loss of enteric ganglia, and neuroblastoma (NB), childhood tumors originating from the sympathetic ganglia and adrenal medulla. The risk for these diseases dramatically increases in patients with congenital central hypoventilation syndrome (CCHS) harboring a nonpolyalanine repeat expansion mutation of the Paired-like homeobox 2b (*PHOX2B*) gene, but the molecular mechanism of pathogenesis remains unknown. We found that introducing nonpolyalanine repeat expansion mutation of the *PHOX2B* into the mouse *Phox2b* locus recapitulates the clinical features of the CCHS associated with HSCR and NB. In mutant embryos, enteric and sympathetic ganglion progenitors showed sustained sex-determining region Y (SRY) box10 (*Sox10*) expression, with impaired proliferation and biased differentiation toward the glial lineage. Nonpolyalanine repeat expansion mutation of PHOX2B reduced transactivation of wild-type PHOX2B on its known target, dopamine β-hydroxylase (DBH), in a dominant-negative fashion. Moreover, the introduced mutation converted the transcriptional effect of PHOX2B on a *Sox10* enhancer from repression to transactivation. Collectively, these data reveal that nonpolyalanine repeat expansion mutation of PHOX2B is both a dominant-negative and gain-of-function mutation. Our results also demonstrate that *Sox10* regulation by PHOX2B is pivotal for the development and pathogenesis of the autonomic ganglia.

Introduction

Neural crest cells (NCCs) are transient and multipotent progenitors that give rise to various cell types, including neural, endocrine, pigment, craniofacial, and conotruncal cardiac cells (1, 2). Impaired development of NCCs causes a wide spectrum of disorders, collectively known as neurocristopathies (3, 4). Most neurocristopathies have a strong genetic basis (5), and investigating how a given genetic change influences NCC behavior is crucial for gaining a better understanding of the pathogenesis of neural crest derivatives, knowledge which will likely be vital to the development of new strategies for the prevention and treatment of neurocristopathy.

Neuroblastoma (NB) and Hirschsprung disease (HSCR) are neurocristopathies of the sympathetic and enteric nervous systems (ENSs). NB arises from the sympathetic ganglia and adrenal medulla and is the most common extracranial malignant tumor in childhood (with an incidence of 10 per 1 million children). NB fatality accounts for 15% of childhood cancer mortality (6–8). HSCR affects 1 in 5,000 live births and is one of the most common intestinal obstructive conditions in neonates (9). The pathology of HSCR is characterized by the absence of the enteric ganglia in the distal part of the gastrointestinal tract. Both NB and HSCR are life-threatening disorders, and the treatment of these diseases demands intensive clinical intervention. Despite the substantial clinical impacts of these diseases, the etiology of NB and HSCR remains poorly understood.

Although NB is a tumor and HSCR is a loss of neural crest derivatives, NB and HSCR occasionally cooccur. This NB-HSCR association is prominent particularly in patients with congenital central hypoventilation syndrome (CCHS; also referred to as *Ondine's curse*), which is a failure in the autonomic control of breathing and is characterized by the absence of the arousal of breathing under hypercapnic or hypoxic conditions (10). The incidence of HSCR and NB is 500- to 1000-fold greater in CCHS patients than in the general population (11, 12).

Recent human genetic studies have identified heterozygous mutations of the Paired-like homeobox 2b (*PHOX2B*) gene in CCHS patients associated with HSCR and NB (12, 13) (hereafter referred to as the CCHS-HSCR-NB association). PHOX2B is a paired homeodomain transcription factor and is essential for the development of cells constituting the autonomic neural circuits (14). The human PHOX2B protein harbors a homeodomain and 2 polyalanine stretches (15), and the amino acid sequences of human PHOX2B are 100% identical to those of the chimpanzee, rat, and mouse, suggesting that the function of PHOX2B is highly conserved in mammals. Although various *PHOX2B* mutations

Conflict of interest: The authors have declared that no conflict of interest exists.
Citation for this article: *J Clin Invest.* 2012;122(9):3145–3158. doi:10.1172/JCI63401.

have been identified in isolated and syndromic cases of CCHS, there are strong correlations between the types of *PHOX2B* mutations and clinical manifestations. Isolated CCHS patients almost exclusively carry mutations that cause an expansion of the second polyalanine repeat (polyalanine repeat expansion mutations [PARMs]) (12, 13). The vast majority of *PHOX2B* mutations identified in CCHS-HSCR-NB association, however, are non-PARMs (NPARM), which are either missense mutations or nucleotide deletions/insertions causing frameshifts of the open reading frame (ORF) (12). Interestingly, in the CCHS-HSCR-NB association, multifocal NB is common (12), suggesting that such mutations affect the sympathetic nervous system globally and are involved in an early phase of tumor development that establishes susceptibility to NB. The evidence collectively suggests that NPARM *PHOX2B* in CCHS-HSCR-NB association exerts a common pathogenic effect on autonomic neural crest derivatives. Elucidation of the function of NPARM *PHOX2B* may thus provide novel insights into autonomic neurocristopathies, HSCR and NB in particular. In this study, we focused on two versions of NPARM *PHOX2B*, and investigated the impact on the development of autonomic ganglia by introducing the NPARM *PHOX2B* into the mouse *Phox2b* locus via gene targeting. We addressed the following issues: (a) whether NPARM *PHOX2B* is sufficient for the expressivity of the disease phenotype; (b) what is the earliest developmental process affected by NPARM *PHOX2B*; and (c) whether there are commonly shared mechanisms underlying the disease phenotype. We show here that NPARM *PHOX2B* mutations affect autonomic ganglion progenitors and cause in mice a phenotype reminiscent of CCHS-HSCR-NB association. We also show that dysregulation of the expression of sex-determining region Y (SRY) box10 (*Sox10*) by NPARM *PHOX2B* is a potentially common factor in the pathogenesis of autonomic neurocristopathy.

Results

Generation of mice harboring human NPARM PHOX2B mutations. Various types of NPARMs in the *PHOX2B* gene have been identified in patients with CCHS-HSCR-NB association. One of the features most frequently shared among those mutations is that they cause a frameshift in the ORF, leading to an addition of aberrant amino acid sequences, which are identical among PHOX2B mutant proteins in the last 42 amino acids of the C-terminal region (Figure 1A). Two of these PHOX2B mutants, 931 del5 and 693–700 del8 (hereafter referred to as del5 and del8, respectively), lack nucleotides 931–935 and 693–700 in the ORF (942 nucleotides), respectively. The nucleotide deletion in del5 occurs in box10, the region close to the stop codon of PHOX2B, while, in del8, the nucleotide deletion occurs between the 2 polyalanine repeat regions, resulting in the absence of a 20-polyalanine repeat in the mutant protein (Figure 1A).

To understand how these NPARM *PHOX2B* mutations affect the development of the nervous system and cause syndromic neurocristopathy, we introduced human genomic fragments of these mutations (extending from the deletion to the new stop codon due to the frameshift) into the mouse *Phox2b* locus by gene targeting (Figure 1B). Homologously recombined ES clones were isolated (Figure 1C), and injection of these clones into blastocysts yielded several chimeric mice. However, all living offspring from these chimeric mice were WT, and only dead newborn heterozygous mice were occasionally found, suggesting that heterozygous del5 and del8 mutations cause lethality soon after birth.

PHOX2B mutant mice recapitulate syndromic neurocristopathy. Perinatal lethality by heterozygous *PHOX2B* mutations was strongly suspected, so we employed intracytoplasmic sperm injection (ICSI) to generate mice heterozygous for del5 and del8 using sperm derived from those chimeric mice (ref. 16; for details see Methods, Supplemental Figure 1, and Supplemental Methods; supplemental material available online with this article; doi:10.1172/JCI63401DS1). This allowed us to examine the phenotype of *Phox2b*$^{del5/+}$ and *Phox2b*$^{del8/+}$ embryos at various developmental time periods, and we confirmed that, in *Phox2b*$^{del5/+}$ and *Phox2b*$^{del8/+}$ embryos, mutant *PHOX2B* was expressed in all tissues that endogenously express the *Phox2b* gene (Figure 1D and data not shown).

Caesarian sections revealed that, at E18.5, *Phox2b*$^{del5/+}$ and *Phox2b*$^{del8/+}$ mice were found at the expected Mendelian ratio, indicating that these mutant embryos develop to term. However, *Phox2b*$^{del5/+}$ and *Phox2b*$^{del8/+}$ mice failed to breathe spontaneously (Figure 2A and Supplemental Video 1). Although breathing could be evoked by skin stimulation, all the mutants died within hours after birth. This phenotype was closely similar to that of mice carrying a 7-polyalanine expansion mutation (PARM) in the *Phox2b* gene (17), the most common genetic hallmark of isolated CCHS.

Histological examination revealed that retrotrapezoid nucleus/parafacial respiratory group (RTN/pFRG) neurons, which make up respiratory centers in the hindbrain, were missing in *Phox2b*$^{del5/+}$ and *Phox2b*$^{del8/+}$ mutants. In addition, other Phox2b-dependent nuclei, including the facial motor nucleus (nVII) and the dorsal motor nucleus of the vagus (dmnX) (18), were less densely populated or nearly absent in these mutants (Figure 2C and Supplemental Figure 2).

Acetylcholinesterase staining of the gut showed that enteric ganglia were noticeably fewer in the colons of *Phox2b*$^{del5/+}$ mice and absent from the colons of *Phox2b*$^{del8/+}$ mice (Figure 2D). In ganglionized gut segments, we detected a decrease of approximately 20%–50% in the numbers of enteric ganglion cells in the mutant gut (WT vs. *del5* vs. *del8*; 100% vs. 79.3% vs. 49.7%). Moreover, the sympathetic ganglia in both mutant mice were smaller and had thinner nerve fibers (Figure 2E) than those in WT mice. Occasionally, sympathetic ganglia of the mutant mice were found in aberrant locations in the sympathetic chain (Figure 2E) and pararenal areas (Figure 2F). All of the above-mentioned phenotypes were more severe in *Phox2b*$^{del8/+}$ than *Phox2b*$^{del5/+}$ mice.

Overt tumor formation was not detected in the sympathetic ganglia and in the adrenal medulla on gross anatomical analysis or H&E staining of sections (data not shown); it was, however, obvious that the entire structure of the sympathetic ganglia was severely affected in the mutant mice. Collectively, introducing human NPARM *PHOX2B* into the mouse *Phox2b* locus resulted in abnormal development of the hindbrain nuclei for respiration and enteric and sympathetic ganglia, demonstrating that *Phox2b*$^{del5/+}$ and *Phox2b*$^{del8/+}$ mice are valuable in vivo tools for studying the molecular mechanisms underlying the CCHS-HSCR-NB association.

NPARM PHOX2B mutations impair neuronal differentiation of the enteric ganglion progenitors. To understand how these *PHOX2B* mutations affect the development of the enteric and sympathetic ganglia, we performed histological analysis of *Phox2b*$^{del5/+}$ and *Phox2b*$^{del8/+}$ embryos.

The ENS is derived from the vagal and sacral NCCs, with much greater contribution of the former than the latter. In mice, the vagal NCCs invade the foregut mesenchyme at about E9.5 (these cells are hereafter called enteric neural crest–derived cells

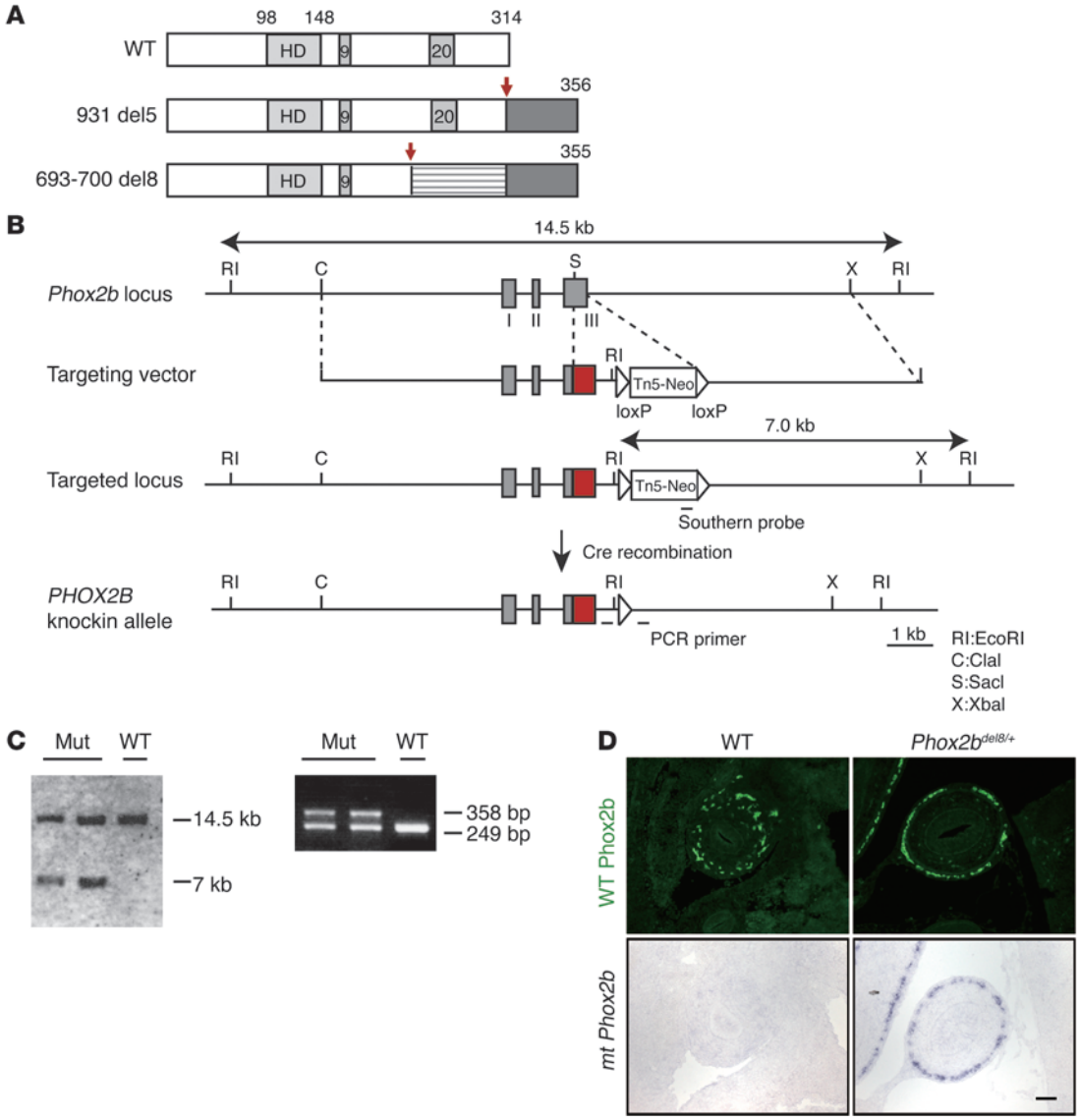

Figure 1

Generation of NPARM *PHOX2B* knockin mice. (**A**) Protein structure of WT and NPARM (931 del5 and 693–700 del8) PHOX2B. Red arrows indicate the regions of the deletions. Dark gray boxes depict aberrant 42 amino acids shared by both del5 and del8 mutant proteins. HD, homeodomain; 9, 20, polyalanine stretches. (**B**) Schematics showing the gene-targeting strategy. Gray boxes indicate exons of the *Phox2b* gene. Red boxes show human genomic fragments spanning from the deletion mutations to the aberrant stop codon due to the shift in the ORF. A floxed (white triangles) Tn5-neo cassette was removed in vivo by Cre recombination. Bars depict the location of the probe for Southern blot analysis and PCR primers for screening the recombined ES clones. (**C**) Southern blot and PCR analysis of WT and the targeted allele of the *Phox2b* gene. Properly targeted ES clones (Mut) display both WT (14.5 kb) and mutant (7 kb) fragments. (**D**) ISH analysis of embryonic gut (E13.5). NPARM *PHOX2B*–specific riboprobes detected signals in enteric ganglion progenitors of del8 mutant but not in WT gut (bottom panels). Anti-WT Phox2b antibodies were used to visualize enteric ganglion progenitors (top panels). Scale bar: 50 μm.

[ENCCs]) and undergo rostral-to-caudal migration within the gut wall until the most advanced ENCCs reach the anal end at E13.5 to E14.0 (1, 19, 20). Phox2b begins to be expressed as soon as ENCCs enter the foregut region (21). During migration, ENCCs proliferate and differentiate in a partially overlapping manner. The state of differentiation can be monitored by the expression of 2 transcription factors, Phox2b and Sox10. Undifferentiated ENCCs express both Phox2b and Sox10 (Phox2b$^+$, Sox10$^+$), whereas cells committed to neuronal or glial differentiation express only Phox2b or Sox10, respectively (22).

In *PHOX2B* mutant embryos, development of the ENS was affected in the mutant gut soon after the onset of *Phox2b* expression. At E10.5, ENCCs were present in the mutant stomach, with the density apparently comparable to that of WT. Immunostaining with anti-Sox10 and WT-specific anti-Phox2b (hereafter described as anti-WT Phox2b) revealed that both proteins were expressed in nearly all ENCCs of both WT and mutant embryos. However, by in situ hybridization (ISH), we found that the levels of Sox10 expression in ENCCs were significantly elevated (Figure 3, A–C; signal intensities of WT, *del5*, and *del8* ENCCs = 1 ± 0.04, 1.19 ± 0.08. and 1.38 ± 0.1;

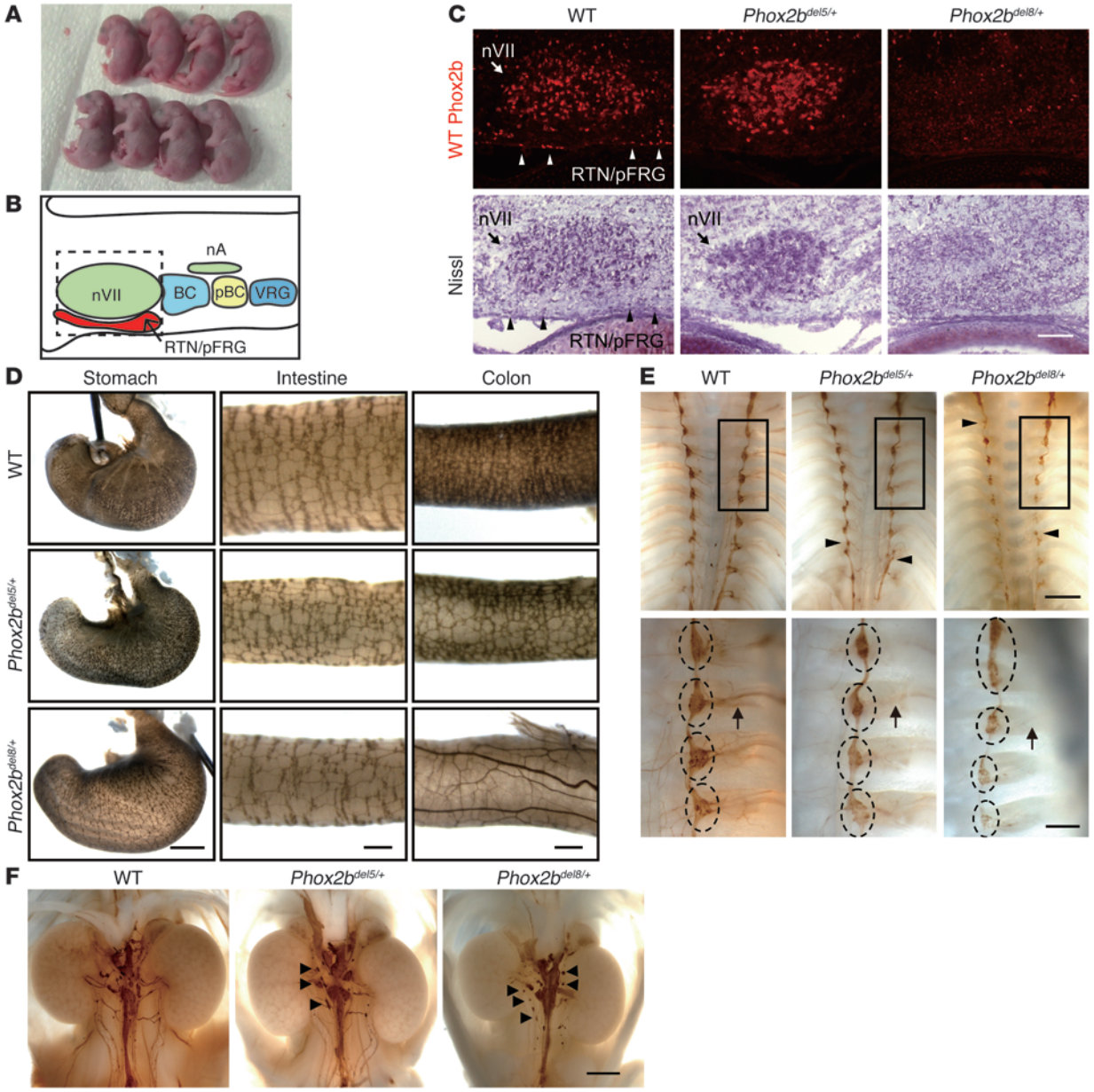

Figure 2

NPARM *PHOX2B* mutant mice display phenotypes reminiscent of CCHS-HSCR-NB association. (**A**) WT (top 4) and del8 mutant (bottom 4) mice born by Caesarian section at E18.5. Note cyanotic skin color of the mutant mice. (**B**) Schematic representation of various brain nuclei in a parasagittal section of the hindbrain. nVII, facial motor nucleus; BC, Bötzinger complex; pBC, pre-Bötzinger complex; VRG, ventral respiratory group. (**C**) Phox2b immunostaining (top) of the hindbrain sections (E18.5) and Nissl staining of the adjacent sections (bottom). Structure of both nVII (arrows) and RTN/pFRG (arrowheads in WT) is severely disrupted in NPARM *PHOX2B* mutant mice. (**D**) Whole-mount acetylcholine esterase staining of the gut. Note the oligoganglionosis and aganglionosis of the colon in del5 and del8 mutant mice, respectively. Thick nerve bundles seen in the colon of del8 mutants are extrinsic nerve fibers that failed to defasciculate due to the absence of the enteric ganglia (61). (**E** and **F**) Whole mount TH staining of the thorax (**E**) and pararenal areas (**F**). Arrowheads indicate aberrantly located ganglia. Note that individual ganglia of the thoracic chain (dotted circles in bottom panels of **E**) of the mutants are smaller in size and harbor thinner nerve fibers than those of WT. Scale bars: 100 μm (**C**, **D** [intestine and colon]); 330 μm (**E** [bottom panels]); 1 mm (**D** [stomach], **E** [top panels], **F**).

P = 0.02 and 0.01 for WT vs. *del5* and for WT vs. *del8*, respectively, 3 embryos examined for each genotype). Sox10 and WT Phox2b double-labeling of the E12.0 gut revealed that ENCCs colonized the entire length of the midgut and a rostral end of the hindgut in WT embryos (Figure 3D). During this period, a delay in gut colonization by mutant ENCCs was readily recognizable in both *Phox2b*$^{del5/+}$ and *Phox2b*$^{del8/+}$ embryos, and this phenotype was more severe in the latter (Figure 3, D-F). The ENCC density of the mutant gut was lower than that of WT (ENCC numbers in ~0.04 mm^2 gut areas; WT vs. *del5* vs. *del8*; 178.9 ± 19.6 vs. 149.0 ± 7.2 vs. 121.5 ± 14.9; n = 3, 1, 3; P = 0.026

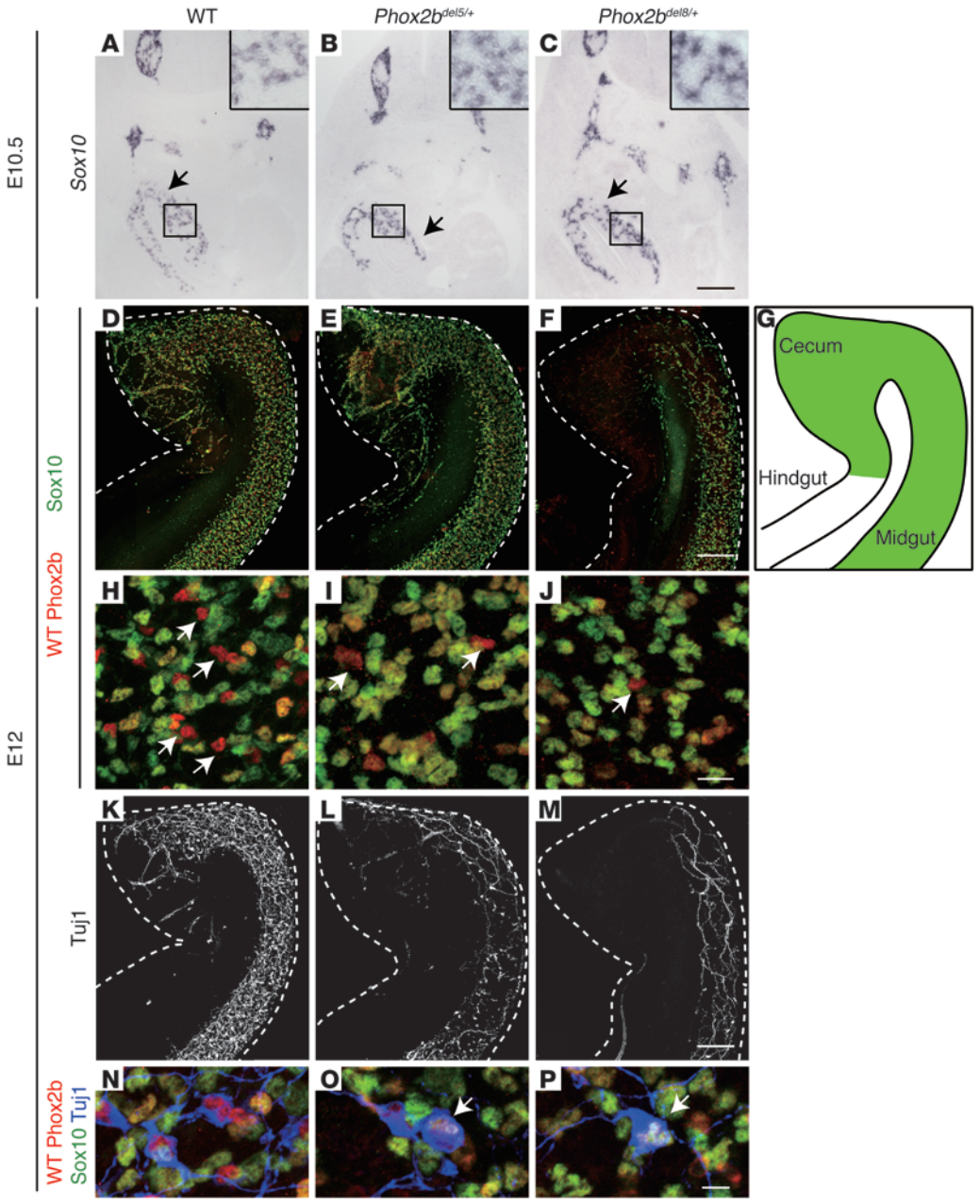

Figure 3

Impaired migration and differentiation of enteric ganglion progenitors in NPARM *PHOX2B* embryos. (**A**–**C**) ISH analysis of Sox10 expression in ENCCs. Arrows indicate the foreguts of E10.5 embryos. Insets in the upper-right corners are larger magnifications of boxed areas. (**D**–**F** and **H**–**J**) Phox2b/Sox10 double immunostaining of E12 gut. Invasion of ENCCs in the hindgut mesenchyme (**D**) is retarded in NPARM *PHOX2B* embryos (**E** and **F**). ENCC density was noticeably lower in the mutant than in WT midgut. (**G**) Schematic representation showing the gut morphology at E12. Areas covered by ENCCs in WT hindgut are shown in green. (**H**–**J**) Larger magnification of the midgut regions. Arrows indicate neuronally committed cells expressing WT Phox2b, but not Sox10. (**K**–**P**) TuJ1 staining of embryonic gut. TuJ1$^+$ cells are drastically decreased in NPARM *PHOX2B* embryos (**L** and **M**). Extinguishment of Sox10 expression in these early differentiating neurons is also impaired in NPARM *PHOX2B* embryos (arrows in **O** and **P**). Scale bars: 10 μm (**P**); 20 μm (**J**); 200 μm (**C**, **F**, and **M**).

for WT and *del8*). To better understand the cause for the decreased ENCC density in NPARM *PHOX2B* mutants, we examined cell death and proliferation. No abnormal cell death was detected in the mutant gut, using anti-activated caspase-3 antibody (Supplemental Figure 3). In contrast 5-ethynyl-2′-deoxyuridine (EdU) (or BrdU) and Phox2b double-labeling revealed that proliferation of mutant ENCCs is compromised at E10 (ratio of double-positive cells in Phox2b-positive cells; WT vs. *del5* vs. *del8*; 51.5% ± 4.2% vs. 43.4% ± 4.2% vs. 39.5% ± 0.95%) and restored at E12 (WT vs. *del5* vs. *del8*; 45.2% ± 1.1% vs. 48.1% ± 4.2% vs. 44.0% ± 6.4%). The data suggest that impaired proliferation of immature ENCCs at E10 is the principal cause for the decreased ENCC density in later developmental stages.

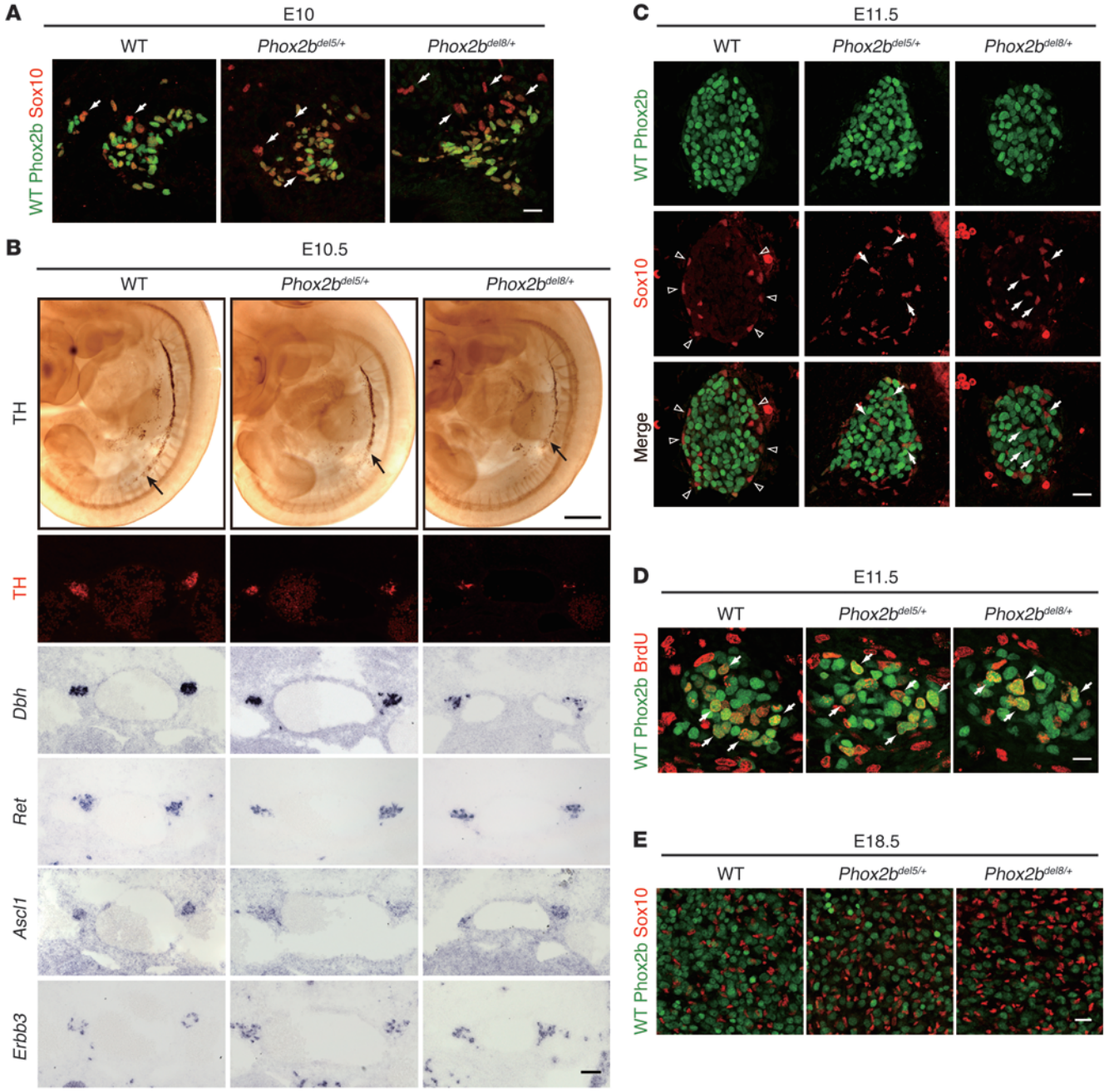

Figure 4

Abnormal neuroglial differentiation of sympathetic ganglion cells in NPARM *PHOX2B* embryos. (**A**) Expression of WT Phox2b and Sox10 in the nascent sympathetic ganglia. Note that Sox10$^+$Phox2b$^-$ cells (white arrows) are more prominent in NPARM *PHOX2B* sympathetic ganglia. (**B**) Expression of various markers in the sympathetic chain. First and second rows represent TH staining of whole-mount preparations and transverse sections of E10.5 embryos. The third through sixth rows show results of ISH analysis. (**C** and **E**) Analysis of neuroglial differentiation in developing sympathetic ganglia by Phox2b/Sox10 immunohistochemistry. Although Sox10$^+$ cells (satellite cell progenitors) are localized preferentially at the periphery of the WT ganglia at E11.5 (**C**, white arrowheads), many Sox10$^+$ cells are also found inside of the sympathetic ganglia in NPARM *PHOX2B* embryos (**C**, arrows). (**D**) BrdU (red) and WT Phox2b (green) double labeling of E11.5 sympathetic chain ganglia. (**E**) Note that, at E18.5, Sox10$^+$ cells appear more prominent in NPARM *PHOX2B* than in WT sympathetic ganglia (SCG). Scale bars: 20 μm (**A**, **C**–**E**); 150 μm (**B**, TH, *Dbh*, *Ret*, *Ascl1*, *Erbb3*); 500 μm (**B**, TH, whole-mount).

At higher magnification of E12 gut, undifferentiated (Phox2b$^+$, Sox10$^+$), neuronal (Phox2b$^+$, Sox10$^-$) and glial (Phox2b$^-$, Sox10$^+$) cells were clearly distinguishable (Figure 3H). This cellular composition was altered in the mutant guts, especially in del8 mutants (Figure 3, I and J); there was a dramatic decrease in neuronal cells (Figure 3, H–J; WT vs. *del8*; 16.5% ± 1.2% vs. 1.7% ± 0.3%, $P = 0.001$) and a corresponding increase in undifferentiated cells (WT vs. *del8*; 59.8% ± 6.9% vs. 77.8% ± 5.3%, $P = 0.02$). The ratio of

Table 1
Counts of neurons and glia in the SCG

	Neuron	Glia	Neuron + glia	Ratio of glia (%)
WT	18236 ± 774.4	7169.0 ± 1012.9	25405.3 ± 1420.6	29.0 ± 2.7
Phox2b$^{del5/+}$	11480 ± 1425.8^{A}	6060 ± 205.6^{B}	17540 ± 1623.8^{C}	35.7 ± 1.8^{D}
Phox2b$^{del8/+}$	2909.3 ± 121.0^{E}	2930.7 ± 258.1^{A}	5840 ± 246.6^{E}	51.1 ± 4.3^{A}

Numbers of neurons and glia were determined by counting the numbers of Phox2b$^+$ and Sox10$^+$ nuclei (see Methods for details). Statistical analysis by Student's *t* test. $^{A}P = 0.002$; $^{B}P < 0.1$; $^{C}P = 0.003$; $^{D}P = 0.02$; $^{E}P < 0.001$.

glial cells, in contrast, did not show any statistically significant differences (WT vs. *del8*; 23.7% ± 6.8% vs. 20.4% ± 5.2%) at this period. Staining of class III β tubulin (TuJ1) to visualize early differentiating neurons revealed fewer neurons in the mutant guts as compared with WT (Figure 3, K–M, TuJ1$^+$ cells in all ENCCs of WT vs. *del5* vs. *del8*; 11.8% vs. 4.0% vs. 1.9%; n = 2, 1, 3). Surprisingly, although Sox10 was no longer expressed in the vast majority of TuJ1$^+$ ENCCs in WT gut, Sox10 was readily detectable in most TuJ1$^+$ cells in the mutant gut (Figure 3, L–P, rate of Sox10$^+$Phox2b$^+$TuJ1$^+$ cells in all TuJ1$^+$ cells; WT vs. *del8*; 6.4% ± 0.6% vs. 63.1% ± 7.3%, P = 0.005), suggesting that downregulation of Sox10 fails to occur in mutant ENCCs. Quantitative RT-PCR using RNAs isolated from E12 gut revealed an increase in *Sox10* expression in mutant gut (WT vs. *del5* vs. *del8*; 1.19 ± 0.13 vs. 1.47 ± 0.32 vs. 1.71 ± 0.14; n = 6, 3, 5; P = 0.03 for WT and *del8*). The estimated total cell numbers of Sox10$^+$ cells in *del8* gut (based on the ENCC density and ratio of Sox10$^+$ cells described above) are less than 80% of those of WT, strongly suggesting that increased Sox10 expression occurs at individual cell levels in mutant ENCCs. These data collectively reveal impaired neuronal differentiation of mutant ENCCs, which is associated with enhanced and sustained expression of *Sox10*.

Unbalanced neuroglial differentiation in NPARM PHOX2B mutant sympathetic ganglia. We also investigated the development of the sympathetic nervous system. Sympathetic ganglia are derived from the trunk NCCs, which migrate in a dorsal-to-ventral fashion around E9.0–E9.5 (23). These NCCs express Sox10, but not Phox2b, during migration (24). Immediately after the completion of migration and formation of the nascent ganglia, Phox2b expression is induced in such ganglion cells (25). From E9.5–E10.5, expression of various genes involved in sympathetic ganglion differentiation commences. By E11.5, the neuronal and glial lineages are segregated, with the former and the latter expressing Phox2b and Sox10, respectively and in a mutually exclusive fashion (26).

Phox2b and Sox10 double staining of the nascent sympathetic ganglia (E10) revealed apparently comparable numbers of ganglion cells between WT and mutant ganglia (Figure 4A; chain ganglia in the lower cervical ~upper thoracic areas) at this time period. No significant difference was detected in proliferation of neuronal progenitors between WT and mutants by EdU/Phox2b double-labeling (EdU$^+$/Phox2b$^+$ cells; WT vs. *del8*; 25.6 ± 5.4% vs. 20.4 ± 3.7%, P = 0.07). Interestingly, however, neuronal progenitors, identified as Phox2b$^+$Sox10$^-$ cells, were significantly decreased, and there was a concomitant increase in undifferentiated (Phox2b$^+$Sox10$^+$) and glial (Phox2b$^-$Sox10$^+$) progenitors in the mutant as compared with WT ganglia (Figure 4A, cervical ~upper thoracic regions of the sympathetic chain). The results suggest that initial neuroglial segregation is already affected in the nascent chain ganglia of NPARM *PHOX2B* mutants.

A decrease in ganglion size was readily discernible at E10.5 and afterwards (Figure 4B and data not shown), especially in del8 mutants. BrdU and Phox2b labeling at E11.5 (Figure 4D) detected significantly fewer double-positive cells in del8 than WT ganglia (WT vs. *del8*; 41.9% ± 5.1% vs. 26.6% ± 3%, P = 0.001), whereas cleaved caspase-3–positive cells were detected neither in WT nor in del8 mutant ganglia (data not shown). Thus, reduction in ganglion size is caused at least partly by the impaired proliferation, but not by reduced survival, of ganglion progenitors. Examination of neuronal and glial markers of the sympathetic ganglia revealed that all of these markers are detectable in the sympathetic chain of E10.5 mutant embryos (Figure 4B). However, cells expressing tyrosine hydroxylase (TH) and dopamine β-hydroxylase (*Dbh*), markers for catecholamine biosynthesis, were noticeably fewer in the mutant than WT ganglia. The difference was less evident with respect to *Ascl1* and *Ret*. This may reflect the physiological expression pattern. Both TH and *Dbh* are expressed in the vast majority of sympathetic ganglion cells (noradrenergic cells) throughout all developmental time periods. In contrast, *Ascl1* is expressed only transiently in early sympathetic ganglion cells (27), and Ret expression is downregulated in the vast majority of ganglion cells after E13.5 (28). That is, markers expressed persistently in differentiated sympathetic neurons were more sensitive in detecting the phenotype of the mutant ganglia. Interestingly, the density of cells expressing *Erbb3*, a glial marker of the sympathetic ganglia at this developmental age, appeared unchanged or slightly expanded in the mutant ganglia. This likely reflects biased differentiation toward the glial lineage, which is initiated as early as E10 (Figure 4A, and see below).

By E11.5, expression of Phox2b and Sox10 was nearly completely segregated in both WT and mutant ganglia. Interestingly, although Sox10$^+$ cells were found almost exclusively at the peripheral margin of WT ganglia (Figure 4C) (26), Sox10$^+$ cells were detected not only at the periphery, but also inside of the mutant ganglia (Figure 4C).

Finally, total numbers of ganglion cells (the superior cervical ganglia [SCG]) were significantly reduced in mutant ganglia at E18.5 (Table 1). Although both neurons (Phox2b$^+$) and glia (Sox10$^+$) were decreased in number, the former were more strongly affected than the latter in mutant ganglia, and the ratio of glial populations in sympathetic ganglia was significantly higher in mutant than in WT ganglia (Figure 4E). No abnormal growth of neuronal and glial cells was observed in NPARM *PHOX2B* mutant mice at this time period (data not shown).

In summary, commitment, proliferation, and differentiation of neuronal progenitors were impaired in the mutant sympathetic ganglia.

NPARM PHOX2B mutants affect self renewal and proliferation of autonomic neural progenitors. The analysis in vivo revealed that autonomic ganglion development is affected soon after the onset of Phox2b expression, demonstrating that mutant NPARM *PHOX2B* initially affects the undifferentiated autonomic neural progenitors. To gain a better understanding of how the behavior of autonomic neural progenitors is altered by NPARM *PHOX2B*, we used neurosphere assays, which allow the examination of self renewal and differentiation capacity of ganglion cell progenitors in vitro (29).

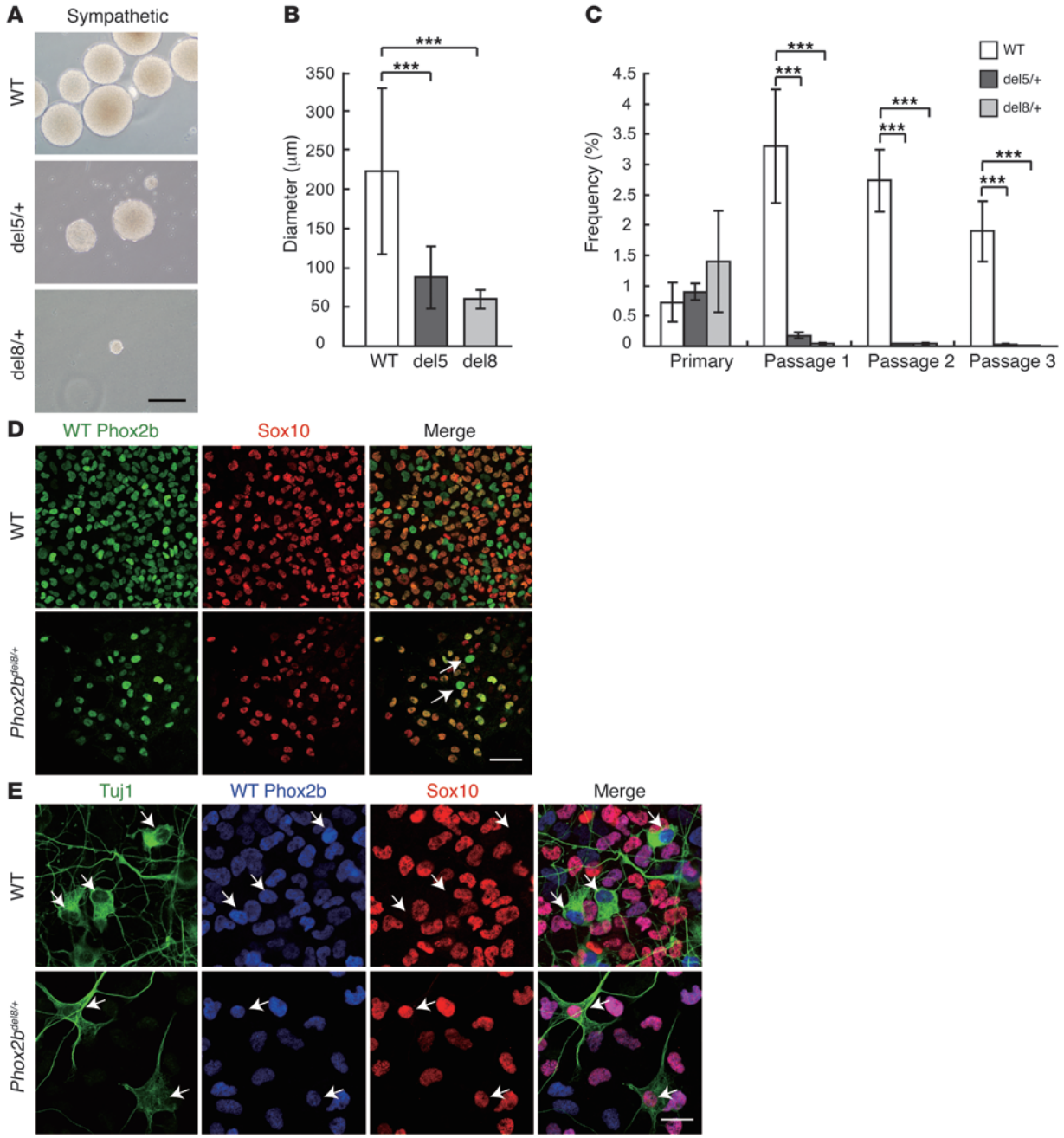

Figure 5

Characterization of the sympathetic ganglion progenitors by a neurosphere method. (**A** and **B**) Morphology and diameter of the primary neurospheres generated from dissociated sympathetic ganglia (E13.5). (**C**) A graph showing neurosphere-forming ability. The numbers of neurospheres generated from 5,000 cells is shown as frequency (%). (**D**) Representative images for Phox2b/Sox10 expression in neurosphere cells cultured on monolayer (passage 1). The vast majority of the NPARM *PHOX2B* mutant–derived neurosphere cells express both Phox2b and Sox10 (bottom panels). Note also that Phox2b$^+$Sox10$^-$ cells are very few in the NPARM *PHOX2B* mutant–derived neurosphere cells (white arrows). (**E**) Immunocytochemical analysis of differentiating neurons (passage 1). TuJ1$^+$ cells derived from NPARM *PHOX2B* neurosphere cells bear thick neurites and aberrantly express Sox10 (white arrows in bottom panels). Scale bars: 20 μm (**E**); 40 μm (**D**); 200 μm (**A**). Error bars indicate SD (n = 3). ***P < 0.001.

The numbers of primary neurospheres generated from the same numbers of dissociated sympathetic ganglion cells did not differ between WT and mutant ganglia (Figure 5C), although the size of mutant-derived neurospheres was much smaller (Figure 5, A and B). Successive passage of WT ganglion-derived neurosphere cells revealed a transient increase in the rate of neurosphere formation (Figure 5C), suggesting that cells capable of forming neurospheres underwent symmetric division. This self-renewal ability was observed even after passage 3, although there was a gradual decline in the self-renewal rate. In stark contrast, mutant

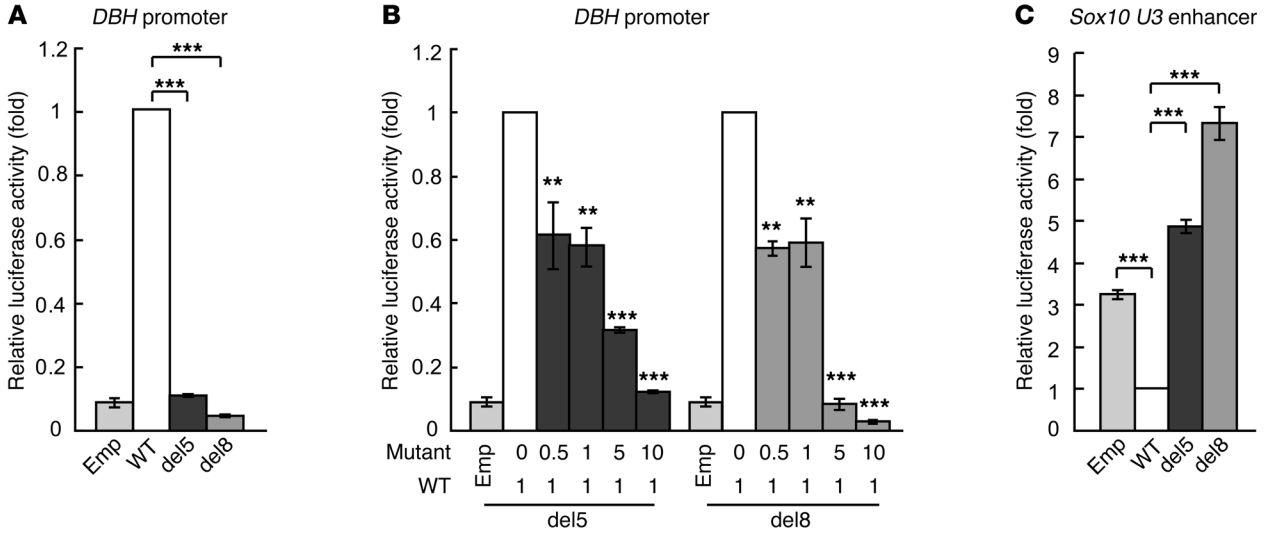

Figure 6

Transcriptional properties of WT and NPARM PHOX2B on *DBH* and *Sox10 U3* reporter genes. Transcriptional activation analysis was performed in NIH3T3 cells using WT and NPARM PHOX2B expression constructs along with *DBH* or *Sox10 U3* reporter genes. (**A**) Transactivation of the *DBH* reporter gene. (**B**) Interaction between WT and NPARM PHOX2B on the *DBH* reporter activation. Transactivation of the *DBH* with a constant amount of WT PHOX2B expression construct and increasing amounts of NPARM PHOX2B expression constructs (from 1:0 to 1:10). (**C**) Effects of WT and NPARM PHOX2B on *U3* enhancer of the *Sox10* gene. Error bars indicate SD ($n = 3$). $^{**}P < 0.01$; $^{***}P < 0.001$.

ganglion-derived neurosphere cells displayed a dramatic decrease in neurosphere-forming ability after the first passage (Figure 5C), indicating that NPARM *PHOX2B* impairs the ability to self renew in sympathetic neural progenitors.

On fibronectin-coated dishes, similar to the aforementioned floating culture conditions, neurosphere cells from mutant ganglia grew much more slowly than those from WT ganglia and were almost unable to passage. The impaired expansion of mutant-derived neurospheres was at least partially accounted for by reduced cell division, as pH3 staining revealed significant differences in the numbers of the stained cells ($pH3^+$ cells/total cells; WT vs. *del8*; 18.2% ± 3.7% vs. 8.8% ± 1.7%; $P < 0.001$).

Phox2b and Sox10 double-immunostaining revealed that neurosphere cells derived from WT ganglia (passage 1) were composed mainly of 3 populations; i.e., $Phox2b^+Sox10^+$ (60.1% ± 8.32%), $Phox2b^+Sox10^-$ (34.8% ± 9.0%), and $Phox2b^-Sox10^+$ (5.0% ± 2.8%) cells (Figure 5D). In striking contrast, nearly all neurosphere cells derived from mutant ganglia expressed Sox10, and the $Phox2b^+Sox10^-$ population (Figure 5D) was dramatically decreased in size ($Phox2b^+Sox10^+$ [64.4% ± 11.1%], $Phox2b^+Sox10^-$ [8.3% ± 7.1%] and $Phox2b^-Sox10^+$ [27.2% ± 7.4%]; Figure 5D), suggesting impaired neuronal differentiation. TuJ1 staining revealed young differentiating neurons with octagonal cell bodies and thin neurites in WT ganglion-derived neurosphere cells. These neurons expressed Phox2b, but not Sox10 (Figure 5E). In contrast, $TuJ1^+$ cells observed in mutant ganglion-derived neurosphere cells had flatter cell bodies, and their neurites appeared thicker and shorter. Surprisingly, many of these TuJ1-expressing cells retained Sox10 expression (Figure 5E). Similar results were obtained from the analysis of gut-derived neurosphere cells (Supplemental Figure 4). In summary, NPARM *PHOX2B* affected self renewal, proliferation, and neuronal differentiation of autonomic neural progenitors, which was associated with abnormally persistent expression of Sox10.

Altered transcriptional properties in NPARM PHOX2B. As with the case of many transcription factors, PHOX2B's transcriptional function changes in a context-dependent manner. For instance, while PHOX2B typically directly binds and activates *DBH* promoter (30), overexpression of Phox2b in neural crest stem cells represses Sox10 expression (31). Our analysis revealed that expression of *DBH* and *Sox10* is dramatically altered in embryos heterozygous for NPARM *PHOX2B*. PHOX2B mutant protein may, therefore, affect expression of *DBH* and *Sox10* by changing the transcriptional activity of the WT *PHOX2B* allele or by acting directly on the cis-regulatory elements of these genes or both. In order to understand the mode of gene regulation by mutant PHOX2B, we employed a luciferase reporter assay using expression constructs for WT and mutant PHOX2B and promoter/enhancer regions of the *DBH* or *Sox10* in NIH3T3 cells, which do not express either of these genes.

Consistent with previous reports (30), transfection of WT PHOX2B significantly transactivated the *DBH* reporter. Such transactivation capacity, however, was abrogated by the mutations (Figure 6A). In order to test whether mutant PHOX2B influences the transactivation capacity of WT PHOX2B, we transfected NIH3T3 cells with a constant amount of WT PHOX2B along with varying concentrations of mutant PHOX2B, and assayed for transactivation of the *DBH*-luciferase reporter gene. Expression and amounts of WT and NPARM PHOX2B proteins in this experimental setting were also examined by Western blot analysis (Supplemental Figure 5). Although both WT and NPARM PHOX2B proteins were clearly detectable, the amount of NPARM PHOX2B was 22%–26% of that of WT PHOX2B (lanes 1, 2 and 7, 8), suggesting that NPARM PHOX2B is less stable than WT PHOX2B. Nonetheless, we found that reporter activity was significantly reduced in a dose-dependent fashion (Figure 6B). The inhibitory effect by NPARM PHOX2B was evident even when protein expression levels of NPARM PHOX2B did not reach that of WT PHOX2B (Figure 6B and Supplemental Figure 5, lanes 3, 4 and 9, 10). Mutant PHOX2B,

therefore, not only loses the ability to transactivate the *DBH* promoter, but also interferes with the transactivation capacity of WT PHOX2B in a dominant negative manner.

Expression of *Sox10* is regulated by several cis-regulatory elements that are conserved across multiple species. Among such conserved sequences, we first selected the *U3* enhancer, which is sufficient for driving gene expression in both mice and fish, in a pattern that recapitulates that of endogenous *Sox10* expression (32, 33). Cells were transfected with *U3*-luciferase construct with either WT or mutant PHOX2B. Interestingly, transfection of WT PHOX2B significantly decreased the luciferase activity of *U3* as compared with control (Figure 6C), indicating that WT PHOX2B acts as a repressor via the *U3* enhancer. Remarkably, both del5 and del8 PHOX2B mutants showed a significant increase in luciferase activity, even as compared with mock-transfected controls, indicating that mutant PHOX2B acts as a transactivator via *U3*. Levels of transactivation were significantly higher in del8 than in del5 mutants, showing a correlation between transactivating capacity and phenotype severity in NPARM *PHOX2B* mutant mice. We further examined whether mutant PHOX2B inhibits repressive action of WT PHOX2B on *U3* enhancer. Repressive action of WT PHOX2B was reversed by increased amount of mutant PHOX2B in a dose-dependent fashion (Supplemental Figure 6). This disinhibition was already significant at a 1:1 ratio of WT and del8 mutant DNA (Supplemental Figure 6; see also Supplemental Figure 5 as the reference for protein levels).

We also examined transcriptional effects of PHOX2B on the other *Sox10* enhancers. Similar to *U3*, NPARM PHOX2B transactivated *Sox10 U1* and *U2* enhancers (refs. 31, 32, Supplemental Figure 7A, and data not shown). In the presence of WT PHOX2B, however, the transactivation effects by NPARM PHOX2B via *U1* enhancer were not as strong as those on *U3* (Supplemental Figure 7B). Transcriptional repression by WT PHOX2B was not observed on *Sox10 U2* enhancer (data not shown), suggesting that transcription of *Sox10* via this enhancer is not regulated in a competitive manner by WT and NPARM PHOX2B.

Collectively, we conclude that mutant PHOX2B acts as both dominant negative and gain-of-function, leading to impaired neuronal differentiation and dysregulation of Sox10 expression.

Discussion

Neurocristopathies in the autonomic nervous system, including HSCR and NB, are one of the most common forms of developmental disorder in pediatric practice, but the exact pathogenic mechanisms underlying these conditions remain elusive. By introducing nonpolyalanine expansion mutations of the *PHOX2B* gene, which were identified specifically in CCHS-HSCR-NB association, into the mouse *Phox2b* locus, we examined the biological influences of these mutations on development of the murine nervous system. Mice heterozygous for NPARM *PHOX2B* died at birth due to lack of spontaneous breathing, a phenotype reminiscent of CCHS. Histological examination revealed that the RTN, a respiratory center in the brainstem, was absent. These mutant mice also displayed HSCR-like distal colon aganglionosis and size reduction and ectopic formation of the sympathetic ganglia. Thus, introduction of NPARM *PHOX2B* affects development of an identical set of neuronal populations in human and mouse, revealing that the pathogenic effects of NPARM *PHOX2B* are significantly conserved in mammals. Investigation of the earliest developmental event affected by these mutations led to the identification of *Sox10* dysregulation as a potentially common cause for HSCR-NB association. This study reports for the first time, to our knowledge, the biological impact of NPARM *PHOX2B* in vivo, and the strikingly conserved pathogenic effects in NPARM *PHOX2B* mutant mice underscores the power of mouse genetic approaches for exploring mechanisms underlying human diseases.

Functional impairment of PHOX2B mutant proteins. PARMs of the *PHOX2B* gene are found in the vast majority of isolated CCHS cases, whereas NPARMs (including del5 and del8) are much more common in CCHS with HSCR and/or NB (12, 13). Our study delineates the functional differences between PARM and NPARM PHOX2B in the physiological context. Mice carrying PARM in the *Phox2b* gene display respiratory distress with selective loss of RTN/pFRG neurons (17). Mice with NPARM *PHOX2B*, in contrast, exhibit deficits in a much broader range of neuronal populations (autonomic ganglia, nVII, and dmnX). This can be accounted for, at least in part, by differences in the transcriptional properties of these Phox2b mutants. For instance, although PARM and NPARM PHOX2B fail to transactivate the *DBH* promoter, the dominant-negative effect of NPARM PHOX2B on WT PHOX2B is much stronger than that of PARM PHOX2B (ref. 34 and this study). Furthermore, the NPARM PHOX2B we examined (del5 and del8) acquired an ability to transactivate *Sox10* via its enhancers. Collectively, the data suggests that NPARM PHOX2B exerts more detrimental effects on the nervous system development than PARM by a combination of dominant-negative and gain-of-function effects.

Notably, the del5 mutant protein retains 98% of the amino acid sequences of WT PHOX2B. This suggests that the alterations in transcriptional activity of del5 are largely attributed to the C-terminal 42 amino acids aberrantly generated by ORF frameshift. It therefore seems reasonable to speculate that these aberrant sequences can recruit, via the C-terminal region, cotransactivators or corepressors, which do not interact with WT PHOX2B.

Finally, although sustained *Sox10* expression by del5 and del8 is a potential cause of impaired autonomic ganglion development, this mechanism does not apply to the deficits in the brain nuclei, as we were not able to detect aberrant Sox10 expression in Phox2b-expressing cells in the hindbrain. Although it remains unknown whether del5 and del8 can transactivate genes other than *Sox10* in these cells, our preliminary data suggest that del8 PHOX2B physically interacts with a set of proteins that do not bind to WT PHOX2B (M. Nagashimada, unpublished observations). Further characterization of the acquired function via aberrant C-terminal sequences will be required to attain a more comprehensive understanding of the molecular basis for CCHS-HSCR-NB association.

Reciprocal regulation between Phox2b and Sox10 is central to development and pathology of the autonomic ganglia. Our in vivo analysis identifies *Sox10* dysregulation as a molecular event shared by developing enteric and sympathetic ganglia of NPARM *PHOX2B* mutant mice and provides insight into the development and pathology of these ganglia (Figure 7). NCCs contributing to these ganglia initially express Sox10, but not Phox2b. Soon after they reach the site of ganglion formation (gut mesenchyme and para/prevertebral areas for the enteric and sympathetic ganglia, respectively), they begin to express Phox2b. These Phox2b/Sox10 double-positive cells are bipotential progenitors whose future identity (either neurons or glia) is as yet undetermined. As differentiation proceeds, Phox2b- and Sox10-expressing cell populations are segre-

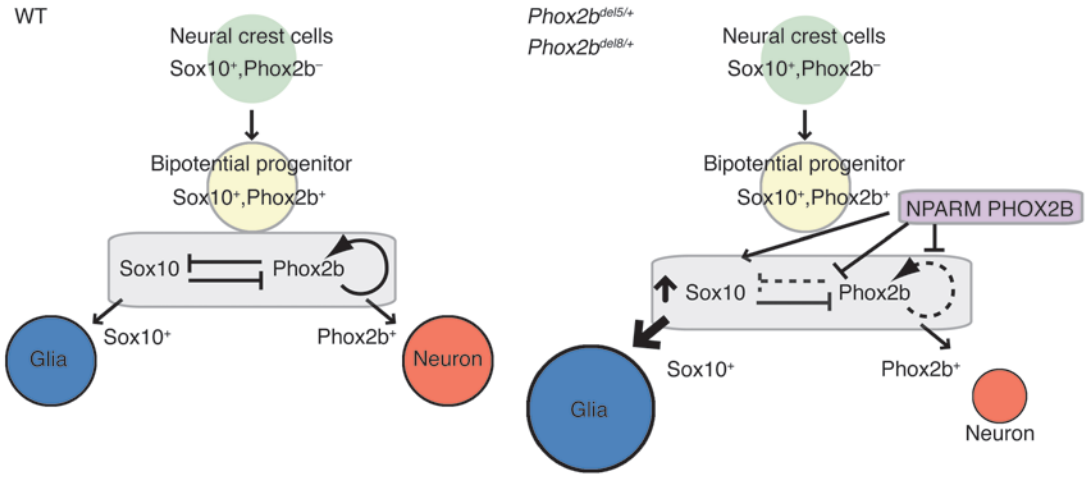

Figure 7

Schematic showing mechanisms underlying autonomic neurocristopathy by NPARM PHOX2B. Regulation Phox2b and Sox10 expression by reciprocal suppression between these 2 transcription factors plays an important role in generating appropriate numbers of neurons and glia in the enteric and sympathetic ganglia (left). NPARM PHOX2B impairs Phox2b's inhibitory activity on Sox10 expression and simultaneously transactivates the *Sox10* gene, leading to biased differentiation of bipotential progenitors toward glial lineage.

gated and contribute to neurons and glia, respectively. The only difference between enteric and sympathetic ganglia with respect to these processes is that Phox2b/Sox10 segregation occurs much earlier and in a shorter time window in the sympathetic than in the enteric ganglion progenitors (E10–E11 and E14.5–E18 for the sympathetic and enteric ganglion progenitors, respectively). Phox2b has the ability to suppress Sox10 expression (ref. 30 and our data) and to increase its own transcription via an autoregulatory loop (35). Sox10 also has the ability to suppress Phox2b expression (31). Together, this reciprocal inhibition between Sox10 and Phox2b must be required to establish a balance between Sox10 and Phox2b expression, which is crucial for the maintenance and differentiation of bipotential progenitors in the sympathetic and enteric ganglia (Figure 7). In the presence of NPARM PHOX2B (Figure 7), the function of WT PHOX2B is suppressed by the mutant protein (see below), resulting in disinhibition and the subsequent upregulation of Sox10 expression. Mutant PHOX2B also can directly upregulate Sox10 expression by acting through its enhancer. These changes shift the balance between Sox10 and Phox2b toward higher levels of Sox10 expression, which leads to biased differentiation toward the glial lineage and a decrease in neuronally differentiated populations.

Development of the ENS requires tight regulation of Sox10 expression. HSCR can occur as an isolated or syndromic trait. Mutations in the *Ret* gene confer predisposition to isolated HSCR, whereas more diverse sets of genes are involved in syndromic HSCR (9). This study identifies an imbalance in Phox2b-Sox10 transcriptional network as one of the potential causes for syndromic HSCR.

Previous studies have shown that maintaining appropriate levels of Sox10 expression is critical for the development of the ENS (36). Our study demonstrates that appropriate downregulation of Sox10 in enteric ganglion progenitors is also important for ENS development. In PHOX2B mutant embryos, abnormally sustained Sox10 expression kept the majority of ENCCs in an undifferentiated state. Those ENCCs, however, were less proliferative than WT ENCCs. The results suggest that, although Sox10 is essential for the maintenance of the progenitor state (31), elevated levels of Sox10 may also exert adverse effects on the proliferation of ENCC, and reciprocal regulation between Sox10 and Phox2b is required for maintaining appropriate levels of Sox10 expression.

The most common surgical intervention for HSCR patients is the removal of an aganglionic gut segment followed by end-to-end anastomosis between the remaining gut and the anus. Some HSCR patients, however, exhibit intestinal problems even after surgery, and defects in the ganglionized gut regions are suspected in those cases (37). NPARM *PHOX2B* mutant mice exhibited paucity in neuronal differentiation and low ENCC density in the ganglionized gut. This implies that structural and functional deficits in the ENS would persist even postnatally in these mice (even if the respiratory problems were rescued) and presumably in patients exhibiting CCHS-HSCR-NB association as well. More careful management of postoperative gastrointestinal function is required for such patients.

Studies in NPARM PHOX2B knockin mice provide novel insight into NB susceptibility. To date, various types of *PHOX2B* mutation have been reported in isolated and syndromic NB cases (12, 38–41). This study provides vital information about how such mutations influence the sympathetic ganglion development in a physiological context. Although our PHOX2B mutant mice displayed severe deficits in development of the sympathetic ganglia, overt tumor formation was not observed, at least at birth. Moreover, we failed to detect increased growth of the PHOX2B mutant sympathetic ganglion cells in any developmental time periods. Rather, sympathetic ganglion progenitors were less proliferative in these mutants. These results appear contrary to the previous observation that overexpression of NPARM *PHOX2B* mutants in chick sympathetic ganglion cells leads to increased proliferation of those cells (42). This may be because different types of NPARM *PHOX2B* mutants were used in that study. Although the precise reason for this discrepancy remains unknown, our mouse genetic system clearly demonstrates that single-copy expression of the NPARM *PHOX2B* allele does not confer growth advantages in sympathetic ganglion progenitors in vivo.

Our neurosphere assay also supports this observation, as the number of secondary neurospheres and the neurosphere diameter, which respectively reflect the self-renewal ability and capacity of

progenitor proliferation, were significantly smaller in mutant than in WT ganglion-derived neurospheres. Given these findings, we conclude that the NPARM *PHOX2B* mutations that we examined are insufficient to support NB formation, at least by birth, and that additional gene mutations must therefore be required for tumors to develop. Should the NPARM *PHOX2B* per se be insufficient for NB tumorigenesis, we nevertheless speculate that NPARM *PHOX2B* does confer NB susceptibility via aberrant expression of Sox10. Several lines of evidence support this hypothesis. First, Sox10 takes part in a program that maintains multipotency in NCCs (31), suggesting that persistent expression of Sox10 can keep cells at least partially in an undifferentiated state. Second, cells in the glial lineage in the peripheral nervous system, or Schwann cell precursors, express Sox10 and are capable of producing multiple cell types (43, 44). They can also be reprogrammed and transdifferentiate (45–47) in response to growth factors (44, 48) or upon injury (49). Given their multipotency and plasticity, glial cells overproduced as a consequence of NPARM *PHOX2B* mutations could be a source of tumors, such as NB. One recent study on a nodular NB discovered that Schwann cells in the tumor were clonal but did not carry mutations found in neuroblastic regions (50). The authors speculate that an initial genetic hit occurs in bipotential progenitors and additional genetic changes in neuronal progenitors, which take place later in development, cause neuroblastic tumors. An alternative possibility based on those data, however, is that initial genetic hit occurs in Schwann cells or their precursors and additional genetic changes inducing dedifferentiation/reprogramming of those cells may lead to the establishment of neuroblastic tumors. In either case, Sox10-expressing cell population appears to play an important role in tumor development.

Although Sox10 expression is detectable in many original tumors of NB patients (51), our preliminary analysis failed to detect Sox10 in the majority of NB cell lines. The exact identity of the Sox10-expressing cell population in the original tumors is currently unknown. More detailed studies on Sox10/PHOX2B expression in NB tumor samples and tumor-initiating cells (52) will be required for future study. We also have to acknowledge, however, the limits of our experimental system, as we are unable to obtain direct evidence indicating the physiological relevance of aberrant Sox10 expression with respect to NB susceptibility. New genetic experiments using a variety of NB mouse models are needed to achieve a better understanding of the contribution of Sox10-expressing cells in the pathogenesis of NB.

Finally, many genetic changes have been reported in HSCR and NB patients, and among these, those with the NAPRM PHOX2B mutation represent only a small fraction (7, 53). Nonetheless, detailed developmental studies of such rare conditions are important, as lower incidence often correlates with higher physiological impact (e.g., mortality) and because multiple types of the causative gene mutations are likely to converge on a common pathway. Future studies of the physiological function of each gene mutation in HSCR and NB using mouse genetic model systems should illuminate the nature of stem cells for the enteric ganglia and of tumor-initiating cells in NB and suggest new strategies for the treatment of these conditions.

Methods

Generation of Phox2b^{del5} and Phox2b^{del8} knockin mice. A WT full-length *PHOX2B* cDNA containing 3′-untranslated region was obtained from human NB cell lines (TGW and NBLS) by PCR. Deletion mutations (931 del5 and 693–700 del8; adenine for the first methionine of PHOX2B cDNA is assigned as 1) were introduced by PCR-based mutagenesis. The targeting vectors were designed such that they introduce the PHOX2B deletion/frameshift mutations, spanning from the deletion to the new stop codon due to the frameshift into the corresponding region of the exon 3 of the *Phox2b* gene. The vectors also contained a neomycin resistance cassette (neo) flanked by loxP sites. Linearized targeting constructs were electroporated into the 129/Ola ES cell line EB3/5 (a gift from Hitoshi Niwa, RIKEN Center for Developmental Biology) (54). G418-resistant clones were screened by Southern blot analysis using an external probe located immediately downstream of the short arm. Properly targeted ES clones were injected into the blastocysts (see Supplemental Methods for more details). All studies were carried out on F2 mice with a hybrid 129/Ola:C57BL/6 or 129/Ola:BDF1 background. Primer sequences for PCR screening of Phox2b$^{del5/+}$ and Phox2b$^{del8/+}$ mice were forward (5′-CTGTCTTGCGGCTCCTCTATAGGA) and reverse (5′-ATCTCTCAGGGCCAAGCGGCTGC), where 249-bp and 358-bp PCR products were amplified for the WT and mutant alleles, respectively.

Histological analysis. ISH, immunohistochemistry, and acetylcholinesterase histochemistry were performed as described elsewhere (55–57). All riboprobes for ISH were synthesized using the DIG RNA Labeling Kit (Roche) as specified by the manufacturer. The primary antibodies used for immunohistochemistry were rabbit anti-Phox2b (1:1000, a gift from J-F. Brunet, CNRS UMR, Paris, France), guinea pig anti-Phox2b (1:500, homemade, raised against the C-terminal region of WT Phox2b [ref. 15]; specificity confirmed by complete overlap of the signals in double staining of mouse embryo sections with rabbit and guinea pig anti-Phox2b antibodies; note that both anti-Phox2b antibodies used in this study recognize only WT Phox2b, as their epitopes are absent in NPARM PHOX2B), goat anti-Sox10 (1:300, Santa Cruz Biotechnology Inc.), sheep anti-TH (1:500, Millipore), and rat anti-BrdU (1:300, Abcam). To detect signals, appropriate secondary antibodies conjugated with Alexa Fluor 488, Alexa Fluor 594, Alexa Fluor 647 (Invitrogen), or Cy3 (Jackson ImmunoResearch Laboratories) were used (1:500).

To examine RTN/pFRG neurons, consecutive parasagittal sections of E18.5 mouse brain were subjected to Phox2b immunohistochemistry and thionin staining. To estimate the numbers of ENCCs at E18.5, guts were subjected to AChE histochemistry. ENCCs were counted in 3 randomly selected areas (0.365 mm^2 each) for each genotype. To quantify signal intensities of *Sox10* transcripts in ENCCs (E10), ISH was performed on consecutive frozen sections of mouse embryos, and color developing was stopped within 6 hours (before saturation of the reaction). Gray-scaled images of ISH photos were inverted to white-on-black, and the signal deposits were quantified by ImageJ (NIH). This method can reveal an increase or decrease in gene expression, although the values may not directly reflect the actual transcript numbers. For the detection of proliferating cells, BrdU (Sigma-Aldrich) or EdU (Invitrogen) was injected intraperitoneally into pregnant mice (6 mg/100 g body weight) 2 hours before dissection. ENCC density in E12 gut was examined by counting the numbers of Sox10$^+$ and/or Phox2b$^+$ nuclei in 3 randomly chosen areas (0.04 mm^2 each). To determine the ratio of Phox2b$^+$ and/or Sox10$^+$ cells in ENCCs of WT and *del8* mutant gut, Sox10$^+$ and/or Phox2b$^+$ nuclei were counted in randomly selected gut areas (700–1700 nuclei were counted for each embryo).

The size of the sympathetic ganglia at E10 was examined by staining consecutive sections (transverse) of embryos with anti-Phox2b and anti-Sox10 antibodies. Areas containing Phox2b$^+$ and/or Sox10$^+$ cells were measured on every third section using ImageJ.

Cell culture. Enteric and sympathetic ganglion progenitors were isolated and cultured as reported previously (58). In brief, cells were isolated from the sympathetic ganglia and gut of E13.5 embryos and cultured in a neurosphere medium (DMEM-low [Gibco; Invitrogen], 20 ng/ml recombi-

nant human bFGF [R&D Systems], 20 ng/ml IGF1 [R&D Systems], 1% N2 supplement [Gibco; Invitrogen], 2% B27 supplement [Gibco; Invitrogen], 50 mM 2-mercaptoethanol, 15% chick embryo extract [ref. 8], 35 μg/ml [110 nM] retinoic acid [Sigma-Aldrich], and penicillin and streptomycin [Meiji]) in nonadhesive culture plates treated with F127 (Sigma-Aldrich). All cultures were maintained at 37°C in 5% CO_2 balanced air.

For immunocytochemical characterization of neurosphere cells, neurospheres were plated on dishes coated with poly-D-lysine (Sigma-Aldrich) and fibronectin (Biomedical Technologies).

For the neurosphere formation assay (nonadherent cultures), 5,000 neurosphere cells were seeded in a 35-mm well, treated with F-127, and cultured for 9–11 days. Frequency of neurosphere formation (%) was calculated by dividing the numbers of neurospheres by 5,000. Proliferation of neurosphere cells was assessed by double immunocytochemistry with rabbit anti-phospho histone H3 (1:1000; Upstate) and anti-Sox10 and/or anti-Phox2b antibodies.

Quantification of Sox10 transcripts in developing gut. Total RNAs were isolated from E12 gut using Trizol (Invitrogen). cDNAs were generated using Superscript III (Invitrogen) and Random Primers (Promega). *Sox10* mRNA levels were analyzed using intron-spanning primers (forward and reverse, 5′-CAGGCTCACTACAAGAGTGC-3′ and 5′-CTTGCCGGACTGCAGCTCTG-3′, respectively) with Power SYBR Green PCR Master Mix (Applied Biosystems) on an ABI 7500 real-time PCR system (Applied Biosystems). Levels of β-actin transcript were used for normalization.

Cell counts of the sympathetic ganglion cells. Mice were perfused with 4% paraformaldehyde, and the SCG were dissected. Consecutive frozen sections (16-μm thickness) of the SCG were stained with anti-Phox2b and anti-Sox10 antibodies, and nuclear profiles were counted in every fourth section. The numbers of neurons and glia were determined by multiplying the total numbers of nuclear profiles positive for Phox2b and Sox10, respectively, by 4. Three mice (E18.5) for each genotype were examined.

Luciferase assay. WT human PHOX2B and mutant (del5 and del8) cDNA were cloned into the pCAGGS expression vector (59). The luciferase reporter constructs containing a 978-bp *DBH* promoter fragment (30) or *Sox10* enhancers (298-bp *U1*, 547-bp *U2* or 396-bp *U3*; alternatively known as *MCS7*, *MCS5* or *MCS4*, respectively) (32, 33) were prepared using pGL3 or pGL4.25 vectors (Promega).

NIH 3T3 cells were seeded at a density of 5.5×10^4 cells in each well of 12-well plates 24 hours before transfection. A DNA mixture consisting of effector (500 ng), luciferase reporter vector (500 ng), and pCS2–β-gal (200 ng) was transfected for 24 hours with Lipofectamine LTX and PLUS (Invitrogen). Lysate preparation, luciferase, and β-gal assays were performed as described (60). Luciferase activities were normalized to β-gal activities. For each experiment, values from 3 samples were averaged and are presented with SD. To confirm expression of WT and NPARM PHOX2B proteins, FLAG-tagged (N-terminal) WT and NPARM PHOX2B expression vectors were constructed and transfected to NIH3T3 cells employing a condition identical to that used for experiments with non–FLAG-tagged constructs. Cell lysates were subjected to Western blot analysis using anti-FLAG (Sigma-Aldrich) and anti–α-tubulin antibody (Sigma-Aldrich).

Study approval. All animal studies were approved by the RIKEN Center for Developmental Biology.

Statistics. Data are presented as mean ± SD. For all experiments, we calculated the difference between groups with 2-tailed Student's *t* test.

Acknowledgments

The authors thank Kazuto Kobayashi for providing genomic fragments of the *DBH* gene. They also thank Hiroshi Sasaki, Ken-ichi Wada, Yohei Yonekura, Toko Kondo, Kaori Hamada, and Chihiro Nishiyama for their excellent technical assistance. This work was supported by RIKEN and MEXT (Grant-in-Aid for Scientific Research on Innovative Areas, Cellular and Molecular Basis for Neuro-Vascular Wiring).

Received for publication February 15, 2012, and accepted in revised form June 21, 2012.

Address correspondence to: Hideki Enomoto, Laboratory for Neuronal Differentiation and Regeneration, RIKEN Center for Developmental Biology, 2-2-3 Minatojima-Minamimachi, Chuo-ku, Kobe, Hyogo 650-0047, Japan. Phone: 81.78.306.3099; Fax: 81.78.306.3089; E-mail: enomoto@cdb.riken.jp.

1. Le Douarin NM. Cell line segregation during peripheral nervous system ontogeny. *Science*. 1986; 231(4745):1515–1522.
2. Le Douarin NM, Kalcheim C. *The Neural Crest*. Cambridge, United Kingdom: Cambridge University Press; 1999.
3. Bolande RP. The neurocristopathies: A unifying concept of disease arising in neural crest. *Hum Pathol*. 1974;5:409–429.
4. Bolande RP. Neurocristopathy: its growth and development in 20 years. *Pediatr Pathol Lab Med*. 1997; 17(1):1–25.
5. Etchevers HC, Amiel J, Lyonnet S. Molecular bases of human neurocristopathies. In: Saint-Jeannet JP, ed. *Neural Crest Induction and Differentiation*. Georgetown, Texas, USA: Landes Bioscience; 2006:213–234.
6. Maris JM, Matthay KK. Molecular biology of neuroblastoma. *J Clin Oncol*. 1999;17(7):2264–2279.
7. Maris JM. Recent advances in neuroblastoma. *N Engl J Med*. 2010;362(23):2202–2211.
8. Janoueix-Lerosey I, Schleiermacher G, Delattre O. Molecular pathogenesis of peripheral neuroblastic tumors. *Oncogene*. 2010;29(11):1566–1579.
9. Amiel J, et al. Hirschsprung disease, associated syndromes and genetics: a review. *J Med Genet*. 2008; 45(1):1–14.
10. Gozal D. Congenital central hypoventilation syndrome: an update. *Pediatr Pulmonol*. 1998; 26(4):273–282.
11. Rohrer T, Trachsel D, Engelcke G, Hammer J. Congenital central hypoventilation syndrome associated with Hirschsprung's disease and neuroblastoma: case of multiple neurocristopathies. *Pediatr Pulmonol*. 2002;33(1):71–76.
12. Trochet D, et al. PHOX2B genotype allows for prediction of tumor risk in congenital central hypoventilation syndrome. *Am J Hum Genet*. 2005; 76(3):421–426.
13. Amiel J, et al. Polyalanine expansion and frameshift mutations of the paired-like homeobox gene PHOX2B in congenital central hypoventilation syndrome. *Nat Genet*. 2003;33(4):459–461.
14. Pattyn A, Morin X, Cremer H, Goridis C, Brunet JF. The homeobox gene Phox2b is essential for the development of autonomic neural crest derivatives. *Nature*. 1999;399(6734):366–370.
15. Pattyn A, Morin X, Cremer H, Goridis C, Brunet JF. Expression and interactions of the two closely related homeobox genes Phox2a and Phox2b during neurogenesis. *Development*. 1997;124(20):4065–4075.
16. Ohta H, Wakayama T. Generation of normal progeny by intracytoplasmic sperm injection following grafting of testicular tissue from cloned mice that died postnatally. *Biol Reprod*. 2005;73(3):390–395.
17. Dubreuil V, et al. A human mutation in Phox2b causes lack of CO2 chemosensitivity, fatal central apnea, and specific loss of parafacial neurons. *Proc Natl Acad Sci U S A*. 2008;105(3):1067–1072.
18. Coppola E, Pattyn A, Guthrie SC, Goridis C, Studer M. Reciprocal gene replacements reveal unique functions for Phox2 genes during neural differentiation. *EMBO J*. 2005;24(24):4392–4403.
19. Yntema CL, Hammond WS. The origin of intrinsic ganglia of trunk viscera from vagal neural crest in the chick embryo. *J Comp Neurol*. 1954;101(2):515–541.
20. Young HM, Hearn CJ, Ciampoli D, Southwell BR, Brunet JF, Newgreen DF. A single rostrocaudal colonization of the rodent intestine by enteric neuron precursors is revealed by the expression of Phox2b, Ret, and p75 and by explants grown under the kidney capsule or in organ culture. *Dev Biol*. 1998; 202(1):67–84.
21. Young HM, Ciampoli D, Hsuan J, Canty AJ. Expression of Ret-, p75(NTR)-, Phox2a-, Phox2b-, and tyrosine hydroxylase-immunoreactivity by undifferentiated neural crest-derived cells and different classes of enteric neurons in the embryonic mouse gut. *Dev Dyn*. 1999;216(2):137–152.
22. Young HM, Bergner AJ, Muller T. Acquisition of neuronal and glial markers by neural crest-derived cells in the mouse intestine. *J Comp Neurol*. 2003; 456(1):1–11.
23. Britsch S, et al. The ErbB2 and ErbB3 receptors and their ligand, neuregulin-1, are essential for development of the sympathetic nervous system. *Genes Dev*. 1998;12(12):1825–1836.
24. Schneider C, Wicht H, Enderich J, Wegner M, Rohrer H. Bone morphogenetic proteins are required in vivo for the generation of sympathetic neurons. *Neuron*. 1999;24(4):861–870.

25. Ernsberger U, Reissmann E, Mason I, Rohrer H. The expression of dopamine beta-hydroxylase, tyrosine hydroxylase, and Phox2 transcription factors in sympathetic neurons: evidence for common regulation during noradrenergic induction and diverging regulation later in development. *Mech Dev*. 2000;92(2):169–177.
26. Callahan T, Young HM, Anderson RB, Enomoto H, Anderson CR. Development of satellite glia in mouse sympathetic ganglia: GDNF and GFR alpha 1 are not essential. *Glia*. 2008;56(13):1428–1437.
27. Lo LC, Johnson JE, Wuenschell CW, Saito T, Anderson DJ. Mammalian achaete-scute homolog 1 is transiently expressed by spatially restricted subsets of early neuroepithelial and neural crest cells. *Genes Dev*. 1991;5(9):1524–1537.
28. Enomoto H, Crawford PA, Gorodinsky A, Heuckeroth RO, Johnson EM, Milbrandt J Jr. RET signaling is essential for migration, axonal growth and axon guidance of developing sympathetic neurons. *Development*. 2001;128(20):3963–3974.
29. Joseph NM, et al. The loss of Nf1 transiently promotes self-renewal but not tumorigenesis by neural crest stem cells. *Cancer Cell*. 2008;13(2):129–140.
30. Seo H, et al. A direct role of the homeodomain proteins Phox2a/2b in noradrenaline neurotransmitter identity determination. *J Neurochem*. 2002; 80(5):905–916.
31. Kim J, Lo L, Dormand E, Anderson DJ. SOX10 maintains multipotency and inhibits neuronal differentiation of neural crest stem cells. *Neuron*. 2003; 38(1):17–31.
32. Werner T, Hammer A, Wahlbuhl M, Bosl MR, Wegner M. Multiple conserved regulatory elements with overlapping functions determine Sox10 expression in mouse embryogenesis. *Nucleic Acids Res*. 2007;35(19):6526–6538.
33. Antonellis A, et al. Identification of neural crest and glial enhancers at the mouse Sox10 locus through transgenesis in zebrafish. *PLoS Genet*. 2008; 4(9):e1000174.
34. Trochet D, et al. Molecular consequences of PHOX2B missense, frameshift and alanine expansion mutations leading to autonomic dysfunction. *Hum Mol Genet*. 2005;14(23):3697–3708.
35. Cargnin F, et al. PHOX2B regulates its own expression by a transcriptional auto-regulatory mechanism. *J Biol Chem*. 2005;280(45):37439–37448.
36. Britsch S, et al. The transcription factor Sox10 is a key regulator of peripheral glial development. *Genes Dev*. 2001;15(1):66–78.
37. Menezes M, Puri P. Long-term outcome of patients with enterocolitis complicating Hirschsprung's disease. *Pediatr Surg Int*. 2006;22(4):316–318.
38. van Limpt V, et al. The Phox2B homeobox gene is mutated in sporadic neuroblastomas. *Oncogene*. 2004; 23(57):9280–9288.
39. Mosse YP, et al. Germline PHOX2B mutation in hereditary neuroblastoma. *Am J Hum Genet*. 2004; 75(4):727–730.
40. Trochet D, et al. Germline mutations of the paired-like homeobox 2B (PHOX2B) gene in neuroblastoma. *Am J Hum Genet*. 2004;74(4):761–764.
41. Perri P, et al. PHOX2B mutations and genetic predisposition to neuroblastoma. *Oncogene*. 2005; 24(18):3050–3053.
42. Reiff T, Tsarovina K, Majdazari A, Schmidt M, del Pino I, Rohrer H. Neuroblastoma phox2b variants stimulate proliferation and dedifferentiation of immature sympathetic neurons. *J Neurosci*. 2010; 30(3):905–915.
43. Morrison SJ, White PM, Zock C, Anderson DJ. Prospective identification, isolation by flow cytometry, and in vivo self-renewal of multipotent mammalian neural crest stem cells. *Cell*. 1999;96(5):737–749.
44. Adameyko I, et al. Schwann cell precursors from nerve innervation are a cellular origin of melanocytes in skin. *Cell*. 2009;139(2):366–379.
45. Dupin E, Real C, Glavieux-Pardanaud C, Vaigot P, Le Douarin NM. Reversal of developmental restrictions in neural crest lineages: transition from Schwann cells to glial-melanocytic precursors in vitro. *Proc Natl Acad Sci U S A*. 2003;100(9):5229–5233.
46. Le Douarin NM, Dupin E. Multipotentiality of the neural crest. *Curr Opin Genet Dev*. 2003; 13(5):529–536.
47. Joseph NM, He S, Quintana E, Kim YG, Nunez G, Morrison SJ. Enteric glia are multipotent in culture but primarily form glia in the adult rodent gut. *J Clin Invest*. 2011;121(9):3398–3411.
48. Widera D, et al. Schwann cells can be reprogrammed to multipotency by culture. *Stem Cells Dev*. 2011;20(12):2053–2064.
49. Laranjeira C, et al. Glial cells in the mouse enteric nervous system can undergo neurogenesis in response to injury. *J Clin Invest*. 2011;121(9):3412–3424.
50. Bourdeaut F, et al. In neuroblastic tumours, Schwann cells do not harbour the genetic alterations of neuroblasts but may nevertheless share the same clonal origin. *Oncogene*. 2008;27(21):3066–3071.
51. Gershon TR, Oppenheimer O, Chin SS, Gerald WL. Temporally regulated neural crest transcription factors distinguish neuroectodermal tumors of varying malignancy and differentiation. *Neoplasia*. 2005; 7(6):575–584.
52. Hansford LM, et al. Neuroblastoma cells isolated from bone marrow metastases contain a naturally enriched tumor-initiating cell. *Cancer Res*. 2007; 67(23):11234–11243.
53. Raabe EH, et al. Prevalence and functional consequence of PHOX2B mutations in neuroblastoma. *Oncogene*. 2008;27(4):469–476.
54. Niwa H, Miyazaki J, Smith AG. Quantitative expression of Oct-3/4 defines differentiation, dedifferentiation or self-renewal of ES cells. *Nat Genet*. 2000;24(4):372–376.
55. Enomoto H, et al. GFRalpha1 expression in cells lacking RET is dispensable for organogenesis and nerve regeneration. *Neuron*. 2004;44(4):623–636.
56. Dauger S, et al. Phox2b controls the development of peripheral chemoreceptors and afferent visceral pathways. *Development*. 2003;130(26):6635–6642.
57. Uesaka T, Jain S, Yonemura S, Uchiyama Y, Milbrandt J, Enomoto H. Conditional ablation of GFRalpha1 in postmigratory enteric neurons triggers unconventional neuronal death in the colon and causes a Hirschsprung's disease phenotype. *Development*. 2007;134(11):2171–2181.
58. Bixby S, Kruger GM, Mosher JT, Joseph NM, Morrison SJ. Cell-intrinsic differences between stem cells from different regions of the peripheral nervous system regulate the generation of neural diversity. *Neuron*. 2002;35(4):643–656.
59. Niwa H, Yamamura K, Miyazaki J. Efficient selection for high-expression transfectants with a novel eukaryotic vector. *Gene*. 1991;108(2):193–199.
60. Sasaki H, Nishizaki Y, Hui C, Nakafuku M, Kondoh H. Regulation of Gli2 and Gli3 activities by an amino-terminal repression domain: implication of Gli2 and Gli3 as primary mediators of Shh signaling. *Development*. 1999;126(17):3915–3924.
61. Enomoto H, et al. GFR a1-deficient mice have deficits in the enteric nervous system and kidneys. *Neuron*. 1998;21(2):317–324.